



## Electron temperature climatology at Millstone Hill and Arecibo

Jiuhou Lei,<sup>1</sup> Raymond G. Roble,<sup>1</sup> Wenbin Wang,<sup>1</sup> Barbara A. Emery,<sup>1</sup>  
and Shun-Rong Zhang<sup>2</sup>

Received 27 August 2006; revised 17 October 2006; accepted 9 November 2006; published 9 February 2007.

[1] In this paper, ionospheric electron temperature ( $T_e$ ) data for more than two solar cycles measured by the incoherent scatter radars (ISR) at Millstone Hill (42.6°N, 71.5°W) and Arecibo (18.3°N, 66.7°W) are compared with the theoretical  $T_e$  calculated from the National Center for Atmospheric Research Thermosphere-Ionosphere-Electrodynamics General Circulation Model (NCAR-TIEGCM) to investigate the temporal variations of  $T_e$ . The comparisons are made for both low and high solar activity conditions and for three seasons: equinox, summer, and winter. The observations show that the diurnal variation of  $T_e$  is characterized by morning and evening peaks at Arecibo and by a morning peak at Millstone Hill. The occurrence and strength of the peaks at Arecibo are significantly different from those at Millstone Hill. Daytime  $T_e$  tends to increase with solar activity at both stations below  $\sim 300$  km.  $T_e$  above 300 km generally decreases with solar activity; however, it increases with solar activity in equinox and summer at Arecibo, whereas it does so only in summer at Millstone Hill. The TIEGCM model can reproduce these variations. However, the modeled evening peak is weaker than that from observations at Arecibo. The simulations show that the daytime bulge of  $T_e$  tends to occur at low latitudes and high solar activity, as seen in the observations, and the significant morning peak at low solar activity over Arecibo is associated with the equatorial anomaly. Moreover, an interesting feature predicted by the model is that the midday  $T_e$  at the  $F_2$  peak height increases with solar activity when  $F_{10.7}$  values are less than about  $100 \times 10^{-22} \text{ W m}^{-2} \text{ Hz}^{-1}$  or larger than  $190 \times 10^{-22} \text{ W m}^{-2} \text{ Hz}^{-1}$  at Millstone Hill; so does at Arecibo when  $F_{10.7}$  values are larger than  $100 \times 10^{-22} \text{ W m}^{-2} \text{ Hz}^{-1}$ . As a result, a positive correlation between daytime  $T_e$  and  $N_e$  occurs under these conditions.

**Citation:** Lei, J., R. G. Roble, W. Wang, B. A. Emery, and S.-R. Zhang (2007), Electron temperature climatology at Millstone Hill and Arecibo, *J. Geophys. Res.*, 112, A02302, doi:10.1029/2006JA012041.

### 1. Introduction

[2] Variations of ionospheric electron temperature ( $T_e$ ) depend on electron density ( $N_e$ ) and the neutral atmosphere both which exhibit noticeable changes under various solar and geophysical conditions. Hence the ionospheric electron temperature also varies with local time, season, solar activity, magnetic activity, altitude, and location [see *Schunk and Nagy*, 1978; *Bilitza*, 1987]. The seasonal and solar activity variations of electron temperature are mostly obtained from satellite observations at fixed altitudes and modeling techniques are used to interpret these observations [e.g., *Brace and Theis*, 1978, 1981; *Su et al.*, 1996; *Watanabe and Oyama*, 1996; *Oyama et al.*, 1996, 1997; *Venkatraman and Heelis*, 1999; *Prabhakaran Nayar et al.*, 2004; *Sharma et al.*, 2005]. In addition to satellite observations, incoherent scatter radar (ISR) is a very powerful,

ground-based remote-probing tool for the study of the ionospheric processes. Since the development of ISR in 1960s, a long-term observational data set has been accumulated and has provided a wealth of information for ionospheric electron temperature. Many researchers have investigated the behavior of ionospheric electron temperature at low and middle latitudes using ISR observations [e.g., *Evans*, 1967, 1973; *Roble*, 1975; *Buonsanto*, 1989; *Fukao et al.*, 1991; *Oliver et al.*, 1991; *Otsuka et al.*, 1998; *Zhang and Holt*, 2004; *Zhang et al.*, 2004].

[3] Morphological studies on seasonal and solar activity variations of electron temperature, especially their altitude and latitude dependence, however, have not yet been made. *Otsuka et al.* [1998] have reported the diurnal, seasonal, and solar cycle variations of ionospheric electron temperature using the middle and upper (MU) atmosphere radar. They found that the occurrence and strength of the morning and evening peaks depend on altitude, season, and solar activity. These peaks basically arise from photoelectron heating of the low-density thermal electron gas; in addition, neutral winds are suggested to play an important role in the formation of the evening peak [*Otsuka et al.*, 1998]. The bottomside  $T_e$  bulge [*Bilitza*, 1987] is also observed by MU. Nevertheless, the seasonal, solar activity, and latitudinal

<sup>1</sup>High Altitude Observatory, National Center for Atmospheric Research, Boulder, Colorado, USA.

<sup>2</sup>Haystack Observatory, Massachusetts Institute of Technology, Westford, Massachusetts, USA.

variations of these peaks and daytime bulge have not been fully understood. Recently, *Zhang and Holt* [2004] and *Zhang et al.* [2004], using the long-term ISR observations over Millstone Hill and St. Santin, also studied variations of ionospheric electron temperatures. They found that solar activity variation of Te and the Te-Ne interrelationship at these two sites exhibit considerable differences, especially in summer. Above 300 km, Te in summer at St. Santin tends to decrease with solar activity. However, the summer Te at Millstone Hill increases with solar activity, and thus a positive correlation between Te and Ne prevails. This feature was also reported by *Bilitza and Hoegy* [1990]. The mechanism for this positive correlation between Te and Ne is, however, not clear.

[4] To date, no systematic comparisons between the observed electron temperatures and the results from theoretical models have been carried out. In this paper we will use both ISR observations (Millstone Hill and Arecibo) and NCAR-TIEGCM simulations to address the following questions about the variations of Te. (1) What is the altitudinal and latitudinal dependence of the morning and evening peaks of Te in different seasons? (2) What are the daytime Te bulge patterns at different latitudes and what does cause the different daytime Te bulge patterns? (3) What are the mechanisms for the increase of Te with solar activity and for the positive correlation between Te and Ne?

## 2. Model Descriptions and Inputs

[5] The model used in this study is the NCAR TIEGCM, which is a three-dimensional, time-dependent model of the thermosphere and ionosphere [e.g., *Richmond et al.*, 1992] that includes neutral wind dynamo effects so that the electric field can be self-consistently solved. Densities of various species are calculated, including N<sub>2</sub>, O<sub>2</sub>, O, N(<sup>4</sup>S), N(<sup>2</sup>D), NO, N<sub>2</sub><sup>+</sup>, O<sup>+</sup>, O<sub>2</sub><sup>+</sup>, NO<sup>+</sup>, and N<sup>+</sup>, along with ion, electron, and neutral temperatures and neutral winds. Recently, diurnal and semidiurnal tidal components from the GSWM [*Hagan et al.*, 1999] are incorporated into the model as perturbations to the lower boundary. A new method for the specification of solar EUV ionization and photoelectron effects has also been included in the most recent version of the model [*Solomon and Qian*, 2005]. The chemistry and rate coefficients used in the model are described in detail by *Roble and Ridley* [1987] and *Roble* [1995] except that the rate coefficients for the O<sup>+</sup>(<sup>4</sup>S) + N<sub>2</sub> and O<sup>+</sup>(<sup>4</sup>S) + O<sub>2</sub> measured by *Hierl et al.* [1997] were used in this study. The model spatial grid is 5° × 5° in latitude/longitude, ranging from -87.5° to +87.5° in latitude and from -180° to +180° in longitude. It has 29 pressure surfaces extending from 97 km to about 500 km at solar minimum (about 700 km at solar maximum) with a vertical resolution of two grid points per scale height and a model time step of 3 min.

[6] In the TIEGCM, the electron energy equation is also solved. The electron energy conservation equation can be expressed in the following form if chemical and viscous heating of the electron gas are neglected [*Schunk and Nagy*, 1978]:

$$\frac{3}{2}n_e k \frac{\partial T_e}{\partial t} = -n_e k T_e \nabla \cdot \vec{u}_e - \frac{3}{2}n_e k \vec{u}_e \nabla \cdot T_e - \nabla \cdot \vec{q}_e + \sum Q_e - \sum L_e \quad (1)$$

where  $k$  is the Boltzmann's constant,  $\vec{u}_e$  is the electron bulk velocity,  $\vec{q}_e$  is the electron heat flow vector expressed as

$$\vec{q}_e = -\beta_e \vec{J} - K_e \nabla T_e \quad (2)$$

$\beta_e$  is the thermoelectric transport coefficient,  $\vec{J}$  is the electric currents, and  $K_e$  is the electron thermal conductivity given by *Banks and Kocharts* [1973]. In the TIEGCM, at present, field-aligned currents are not included in the equation (2), and the adiabatic expansion and heat advection terms in equation (1) are omitted.

[7] In equation (1),  $\sum Q_e$  and  $\sum L_e$  are the sum of all the local electron heating and cooling rates, respectively. The energy sources for electrons include photoelectron and particle precipitation heating. The processes that are effective in cooling the thermal electron gas include elastic collision with neutral particles (N<sub>2</sub>, O<sub>2</sub>, and O), vibrational and rotational excitation of N<sub>2</sub> and O<sub>2</sub>, excitation of the fine structure levels of atomic oxygen, and excitation from <sup>3</sup>P to <sup>1</sup>D state for atomic oxygen, and the energy transfer by electron-ion collisions [see *Schunk and Nagy*, 1978]. The reader is referred to *Wang et al.* [2006] for the detail description about the electron heating and cooling rates in the model.

[8] The electron heat flux at the upper boundary is modified to match the derived heat flux from the ISR observation at Millstone Hill and Arecibo. As seen from Figure 1, the heat flux at 500 km increases with solar activity except for the evening period at Arecibo when an evening peak occurs. This point will be discussed later. The nighttime heat flux is about 5–6 times smaller than the daytime values at Millstone Hill and is even smaller at Arecibo. Thus the heat flux  $F_e$  (in unit of eV cm<sup>-3</sup> s<sup>-1</sup>) is specified as

$$F_e^d = -4 \times 10^7 F_{107} \times A - 2.0 \times 10^7 F_{107} \quad (3)$$

for day and

$$F_e^n = \frac{F_e^d}{B} \quad (4)$$

for night, where A and B represent the latitudinal variations of the heat flux as follows

$$A = 0.5 \left[ 1 + \sin \left( \pi \frac{|\phi_{GM}| - \pi/9}{\pi/4.5} \right) \right] \quad |\phi_{GM}| < \pi/4.5 \quad (5)$$

$$B = 11.9 - 14.1 \phi_{GM}^2$$

$$A = 1$$

$$B = 5$$

$$|\phi_{GM}| \geq \pi/4.5 \quad (6)$$

Note that  $\phi_{GM}$  is the geomagnetic latitude.

[9] Input parameters of the model are cross polar cap potential, hemispheric power and solar flux index ( $F_{107}$ ). In this study, the total hemispheric power of precipitating auroral electrons was 16 GW, and the cross-polar-cap potential was 45 kV to represent geomagnetically quiet conditions [see *Fesen et al.*, 2002]. The solar 10.7-cm radiation flux

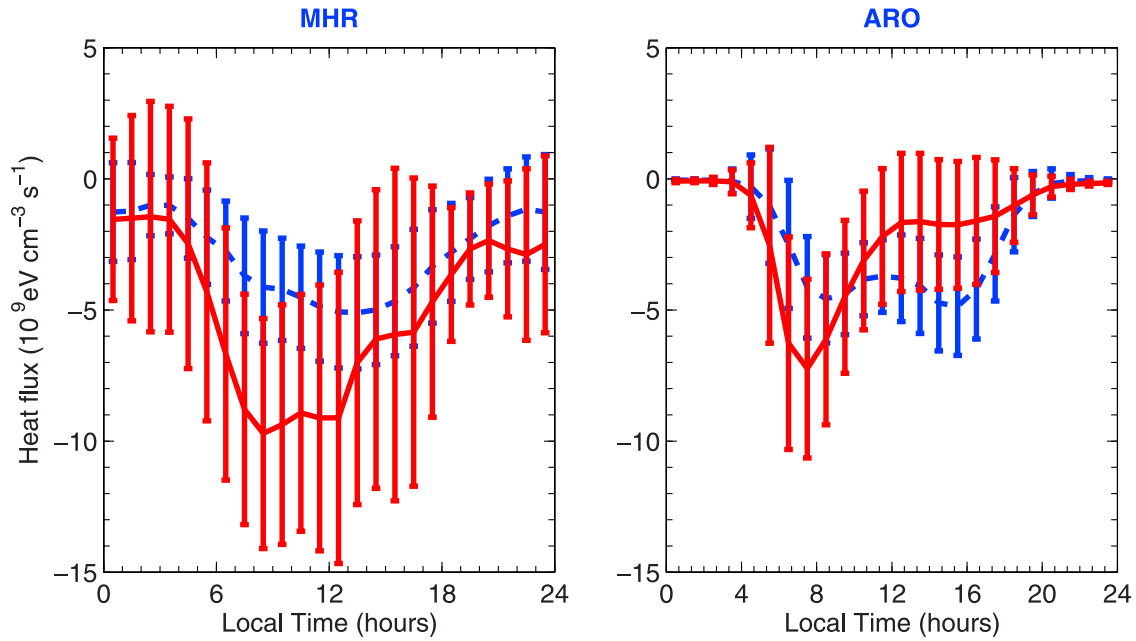


**Figure 1.** The heat flux at 500 km derived from the ISR electron temperature data at (left) Millstone Hill and (right) Arecibo. Note that for each station the data are grouped in low (dashed line;  $F_{10.7} \leq 100 \times 10^{-22} \text{ W m}^{-2} \text{ Hz}^{-1}$ ) and high (solid line;  $F_{10.7} \geq 170 \times 10^{-22} \text{ W m}^{-2} \text{ Hz}^{-1}$ ) solar activity and the error bars show standard deviations.

$F_{10.7}$  was  $80 \times 10^{-22}$  and  $200 \times 10^{-22} \text{ W m}^{-2} \text{ Hz}^{-1}$ , standing for low and high solar activity, respectively. Simulations of the TIEGCM presented here are for 21 March, 21 June, and 21 December to represent northern hemisphere equinox, summer, and winter conditions.

### 3. Data

[10] The ISR data at Millstone Hill are retrieved from the Madrigal database at the Haystack Observatory (<http://www.openmadrigal.org>), and the Arecibo data are retrieved from the CEDAR database (<http://cedarweb.hao.ucar.edu>). The information of these two ISR sites is listed in Table 1.

[11] The Millstone Hill UHF ISR system operates with a zenith-directed 68 m fixed parabolic antenna, which commenced operation in 1963, and a fully steerable 46 m antenna, which commenced operation in 1978. More details about the ISR experiments and the data at Millstone Hill can be seen in the work of *Holt et al.* [2002]. For this study, the zenith measurements for more than two solar cycles (1976–2002) are used. Because each operation program uses different pulse lengths, which are related to the height resolution, data with pulse length  $>480 \mu\text{s}$  for electron

density and  $>640 \mu\text{s}$  for ionospheric temperatures are excluded in this study; thus the data used in this study have pulse length  $300 \mu\text{s}$  or less with a height spacing of better than 22 km.

[12] The 430 MHz ISR at the National Astronomy and Ionosphere Center (NAIC) at Arecibo, Puerto Rico, has made ionospheric measurements since 1963. The Arecibo radar measures many ionospheric parameters, including: line-sight velocity, electron density  $N_e$ , electron temperature  $T_e$ , and ion temperature  $T_i$ . A number of programs have been developed at Arecibo to optimize the observations at different regions and for different parameters. In this paper, we use data from all  $F$ -region programs covering the height range of 140–660 km during the period of 1966–2002.

[13] The ISR observations are grouped into three seasons (equinox, summer, and winter) and two solar flux levels (daily  $F_{10.7} \leq 100 \times 10^{-22} \text{ W m}^{-2} \text{ Hz}^{-1}$  for low solar activity and  $F_{10.7} \geq 170 \times 10^{-22} \text{ W m}^{-2} \text{ Hz}^{-1}$  for high solar activity) in altitude and local time bins. March, April, September, and October are for equinox; June and July are for summer; and December and January are for winter. Data with a daily mean  $A_p$  index greater than 30  $\gamma$  are excluded so as to eliminate geomagnetic activity effects. The average

**Table 1.** ISR Data Used in This Study<sup>a</sup>

Station	Geographic		Geomagnetic Latitude	$F_{10.7}(A_p)$			Year Analyzed
	Latitude	Longitude		Equinox	Summer	Winter	
Millstone Hill	42.6N	71.5W	53.1N	77(13)	77(8)	79(9)	1976–2002
				203(12)	197(11)	199(9)	
Arecibo	18.3N	66.7W	29.0N	76(14)	81(7)	78(13)	1966–2002
				198(11)	192(10)	208(10)	

<sup>a</sup> $F_{10.7}(A_p)$  means the averaged daily solar 10.7-cm solar flux flux (in unit of  $10^{-22} \text{ W m}^{-2} \text{ Hz}^{-1}$ ) and the daily geomagnetic index (in brackets). For each station, there are two rows standing for  $F_{10.7}(A_p)$  at low and high solar activity, respectively.

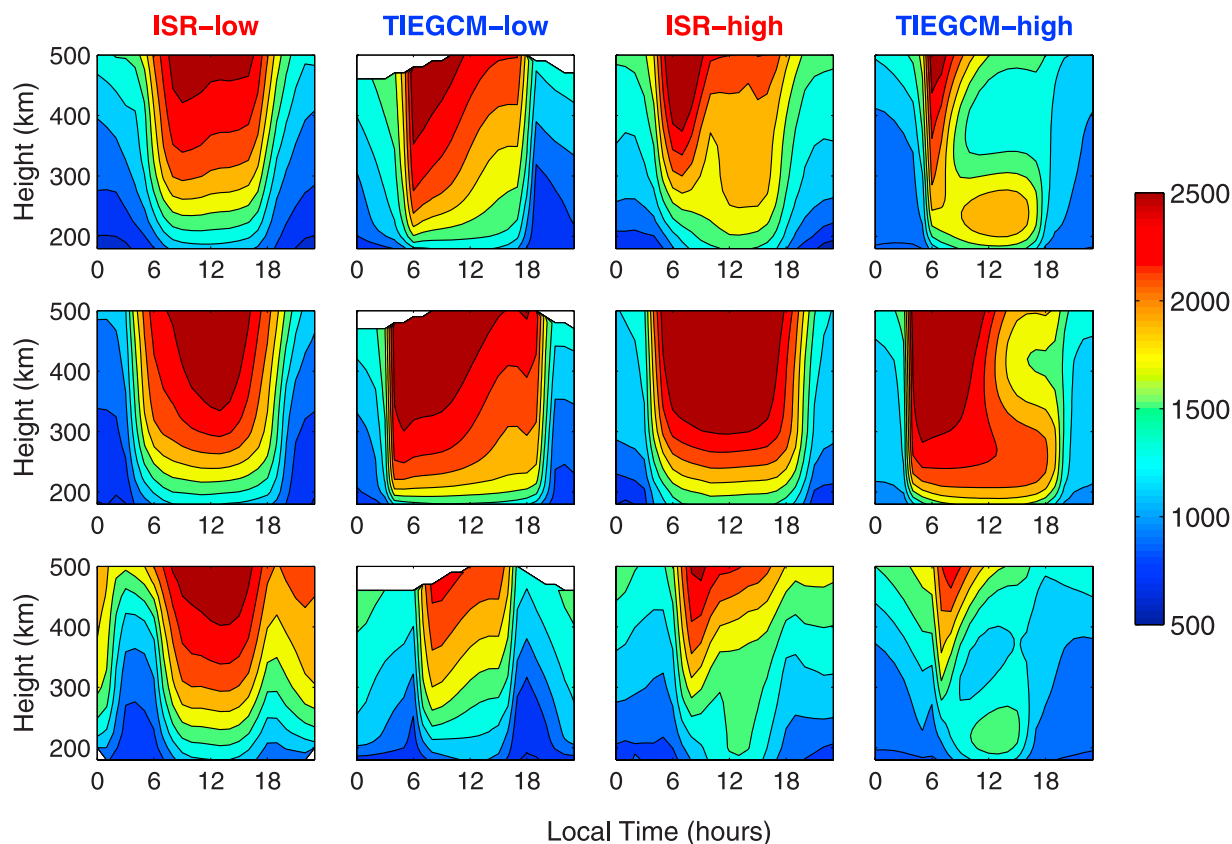


**Figure 2.** Electron temperatures ( $T_e$ , in degrees Kelvin) observed at Millstone Hill and those simulated by the TIEGCM. The plots show from left to right: the ISR data (ISR-low) and the TIEGCM calculations (TIEGCM-low) at low solar activity, the ISR data (ISR-high) and the TIEGCM calculations (TIEGCM-high) at high solar activity; from top to bottom are  $T_e$  for equinox, summer and winter, respectively.

solar flux and magnetic activity conditions are also given in Table 1.

## 4. Results and Discussions

### 4.1. Model/Data Comparisons

[14] Figures 2–3 show comparisons of electron temperature and electron density observed by ISR with those predicted by the TIEGCM at Millstone Hill, respectively; Figures 4–5 are for Arecibo. For each figure, the seasonal variations are arranged from top to bottom for equinox, summer, and winter; the plots are also arranged from left to right for the ISR data (ISR-low) and the TIEGCM calculations (TIEGCM-low) at low solar activity, the ISR data (ISR-high) and the TIEGCM calculations (TIEGCM-high) at high solar activity. It can be seen clearly from Figures 2–5 that the electron temperature and electron density change with local time, altitude, season, solar activity, and latitude in a rather complicated way.

#### 4.1.1. Millstone Hill

[15] The diurnal variation of  $T_e$  is the most significant of all variations because solar radiation at a particular location depends on the solar zenith angle (local time), as shown in Figure 2. The TIEGCM simulated  $T_e$  agrees reasonably well with the observations. For low solar activity, in equinox and summer,  $T_e$  at 300 km increases from about 800 K at night to 2000 K by day. The nighttime  $T_e$  generally tends to equal

the neutral temperature ( $T_n$ ) when the direct solar energy input is absent. In winter, the observed nighttime  $T_e$  above 300 km exceeds 1500 K, which is much higher than that in other seasons, while the modeled  $T_e$  is lower than the observed values by 200–300 K because the model does not include photoelectron heating from the conjugate ionosphere during the Millstone Hill winter night when the magnetic conjugate latitude is in summer and is still under sunlit [Evans, 1973; Schunk and Nagy, 1978; Zhang *et al.*, 2004]. In addition, the relatively low electron density during the winter nighttime (Figure 3) reduces electron energy loss to the ions by collisions and thus also contributes to a larger nighttime  $T_e$  in winter than in other seasons. The modeled daytime  $T_e$  is highest in summer and lowest in winter, as a result of the well-known winter anomaly of Ne at Millstone Hill (Figure 3; also see Lei *et al.* [2005]). Note that there is still significant disagreement between data and model simulations during daytime. The observed  $T_e$  is almost symmetrical around local noon in all seasons, whereas the model gives larger  $T_e$  values in the morning sector than in the afternoon.

[16] For high solar activity, the model reproduces well the sharp morning peak above 250 km in equinox and winter. The morning peak does not occur in the bottomside ionosphere (below 200 km) in any season and at any altitude in summer, as reported by Otsuka *et al.* [1998] from MU observations. It is well known that this morning  $T_e$  peak is

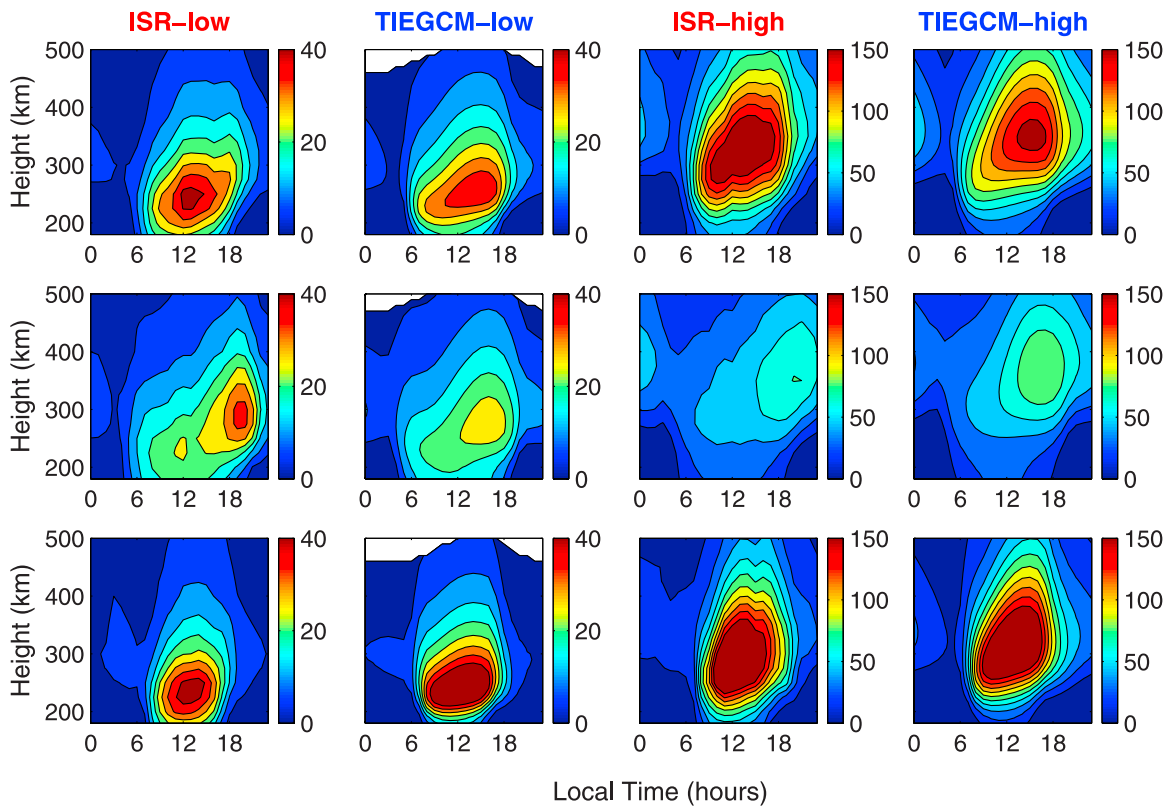


**Figure 3.** Same as Figure 2, except for electron density  $N_e$  (in unit of  $10^{10} \text{ m}^{-3}$ ).

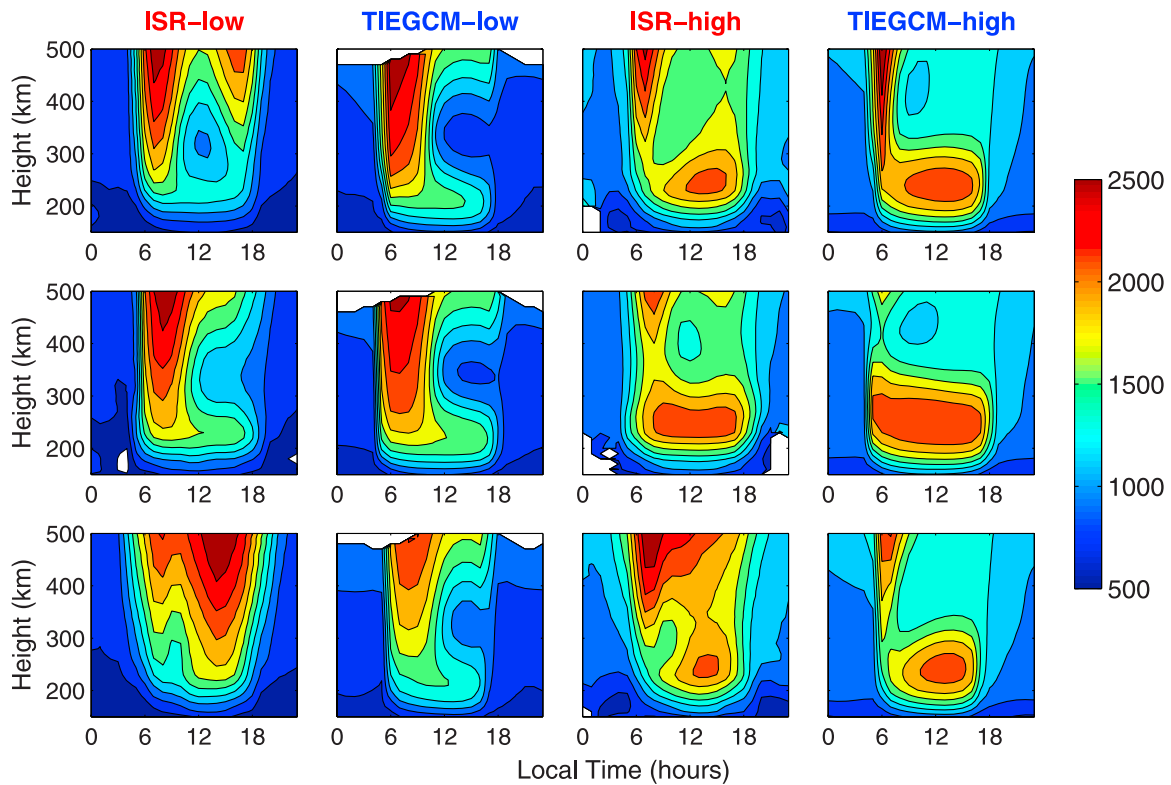


**Figure 4.** Same as Figure 2, but for Arecibo.

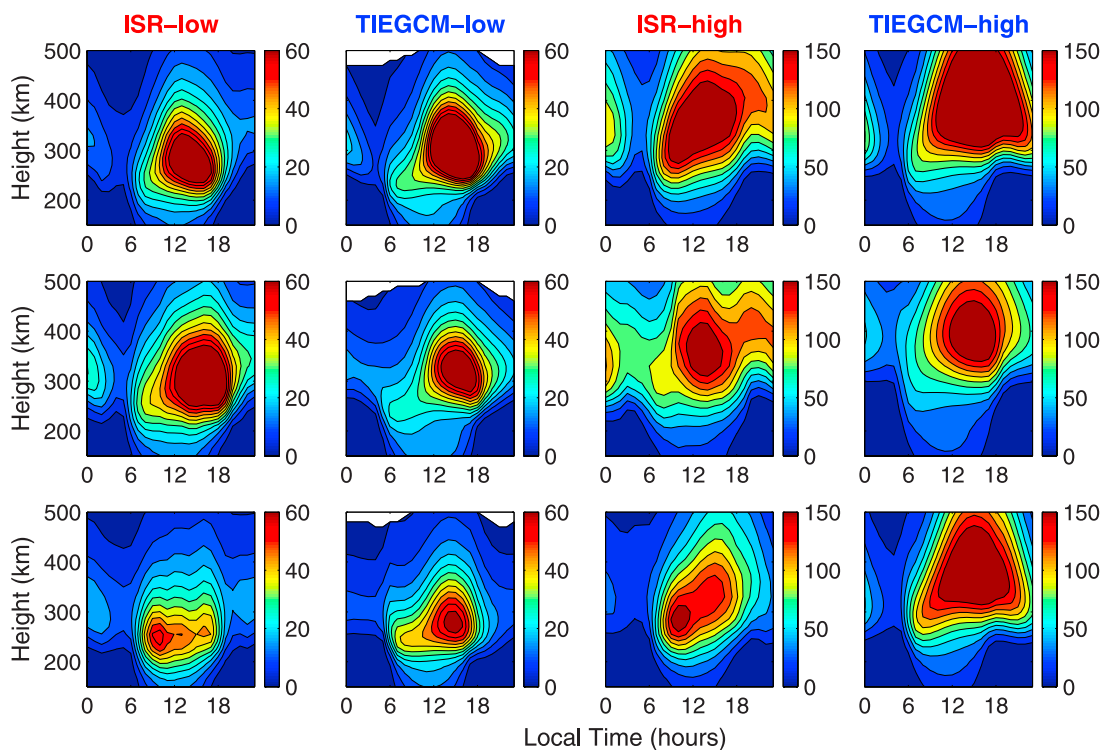


**Figure 5.** Same as Figure 4, except for electron density  $N_e$  (in unit of  $10^{10} \text{ m}^{-3}$ ).

caused by photoelectron heating of the low-density thermal electrons [Dalgarno and McElroy, 1965]. The modeled seasonal variation of  $T_e$  is the same as that from the observations. For instance, both the model and observations show that the daytime  $T_e$  is highest in summer and lowest in winter. However, there are also some differences between the model and observations. The model underestimates  $T_e$  in the afternoon (1500–1800 LT), and gives a stronger daytime bulge of  $T_e$  than the observations.

[17] By comparing variations of  $T_e$  under both low and high solar activity levels, we can examine their solar activity dependence. Results from both the observations and model, however, show that daytime  $T_e$  increases with solar activity at all altitudes in summer and at the bottomside ionosphere in all seasons. At night,  $T_e$  increases with solar activity in equinox and summer; this is caused by the increase of the neutral temperature with solar activity. In winter, however, the modeled nighttime  $T_e$  decreases with solar activity, which is similar but not as significant as the observations; this is partially due to neglecting the effect of the conjugate photoelectron heating in the model, as noted earlier.

#### 4.1.2. Arecibo

[18] As shown in Figure 4, excellent agreement between the simulations and the observations is obtained for  $T_e$  at Arecibo under both low and high solar activity conditions. Note that the daytime  $T_e$  at Arecibo is much lower than that at Millstone Hill because of larger electron density and less heat conduction at Arecibo. The heat conduction is much smaller at Arecibo due to its smaller magnetic dip angle ( $I$ ) of  $49.7^\circ$  relative to the magnetic dip angle of  $72^\circ$  at Millstone Hill, since the heat conduction is proportional to  $\sin^2 I$ .

[19] For low solar activity, the most striking feature of the ISR observations is the morning peak in all seasons and the evening peak in equinox and winter. The large  $T_e$  in the

afternoon sector in winter corresponds with low electron density (Figure 5). These results are different from those at Millstone Hill and MU. At Millstone Hill, the morning and evening peaks are almost absent at low solar activity; at MU, the morning peak does not occur in summer [Otsuka *et al.*, 1998]. The model reproduces well the morning peak; however, the model gives a much weaker evening peak. The seasonal variation of daytime ISR  $T_e$  changes with local time. For example, in the morning sector  $T_e$  is highest in summer, whereas in the afternoon it is highest in winter. The modeled  $T_e$  is in general agreement with the observation in the morning sector, but it does not show the observed significant seasonal variations in the afternoon sector, as a result of the weak evening peak in the model. During the night, both the model and data show that  $T_e$  almost does not have any seasonal variation, whereas at Millstone Hill, the winter night  $T_e$  is obviously larger than that in other seasons because of the conjugate photoelectron heating. The magnetic conjugate point for Arecibo, however, is at much lower latitude and the conjugate photoelectron heating thus becomes negligible; thus the  $T_e$  enhancement does not occur. This is similar to that for St. Santin [Zhang *et al.*, 2004].

[20] For high solar activity, good agreement between the observations and the model can be seen at Arecibo. Differences between the modeled and observed  $T_e$  are about 100 K in equinox and summer, within the range of the standard deviations (not shown); a major discrepancy occurs above 350 km during the daytime when the modeled  $N_e$  is higher than the observed (Figure 5). In addition to the morning peak, another striking feature caught by the model is the daytime  $T_e$  bulge. The daytime  $T_e$  bulge is characterized by a temperature maximum at altitudes between about 200 and 300 km and then a temperature decrease. The strength and

its occurrence of the daytime bulge also vary with season, solar activity, and latitude. As seen in Figure 4, the daytime bulge is most prominent at high solar activity and is strongest in summer and weakest in winter at Arecibo. Again, day-night differences are larger at the altitudes where the daytime bulge occurs, which is similar to that observed by MU [Otsuka *et al.*, 1998]. The seasonal variation of the daytime Te changes with altitude. Below 300 km, the modeled Te is higher in summer and lower in winter, the same as those obtained by the observations; above this altitude, the model also predicts higher Te in winter than in others seasons, except that the modeled values are lower than the observed ones.

[21] It can be seen from Figure 4 that the nighttime Te generally increases with solar activity while the daytime Te changes in a complex way. The daytime Te tends to increase with the solar activity below the F<sub>2</sub> peak height, the same as that at Millstone Hill; the slope of Te with the solar activity, however, is larger than that at Millstone Hill because the daytime bulge of Te is much stronger at Arecibo. Above 300 km, except for the morning period, the daytime Te increases slightly with solar activity in both equinox and summer, while at Millstone Hill this situation only occurs in summer.

#### 4.2. Te-Ne Interrelationship

[22] The anticorrelations between Te and Ne are widely applied to develop empirical Te models [e.g., Bilitza, 1975; Mahajan, 1977]; however, as discussed above, under some conditions a positive correlation between Te and Ne occurs at Millstone Hill and Arecibo. In fact, the competing process between the electron heating rate (proportional to Ne) and the electron cooling rate (proportional to Ne<sup>2</sup>) determines the solar activity dependence of Te [see Otsuka *et al.*, 1998]. Apparently, solar activity variation of Te should depend on background Ne. Zhang *et al.* [2004] suggested that there exists a Ne threshold to turn on or off its effect on Te. We will present simulations to support this conclusion. We performed a series of runs under different F<sub>10.7</sub> values between  $60 \times 10^{-22}$  and  $240 \times 10^{-22}$  W m<sup>-2</sup> Hz<sup>-1</sup> with an increment of  $10 \times 10^{-22}$  W m<sup>-2</sup> Hz<sup>-1</sup> in equinox; all other inputs and conditions are identical to those described in section 2.

[23] Figure 6 shows variations of daytime Ne and Te with F<sub>10.7</sub> at the F<sub>2</sub> peak height at Millstone Hill. It is evident that Ne increases with solar activity with varying slope. It should be noted that ISR and other observations [e.g., Lei *et al.*, 2005, and references therein] suggested that a saturation in electron density occurs when F<sub>10.7</sub> is greater than  $200 \times 10^{-22}$  W m<sup>-2</sup> Hz<sup>-1</sup>, but the model does not predict the same level of saturation seen in the observations. This may be related to the linear relationship between the solar EUV flux and the F<sub>10.7</sub> index used in the TIEGCM model [Solomon and Qian, 2005]. (Note that the saturation effect in electron density at the fixed height, for example, 300 km, is much more significant; see J. Lei *et al.*, A simulation study of thermospheric neutral winds over the MU radar, submitted to *Journal of Geophysical Research*, 2006). Figure 6 shows that Te variations are very complicated. When F<sub>10.7</sub> is less than  $100 \times 10^{-22}$  W m<sup>-2</sup> Hz<sup>-1</sup>, Te tends to increase with solar activity, since electron cooling rate due to Coulomb collisions between the electrons and the

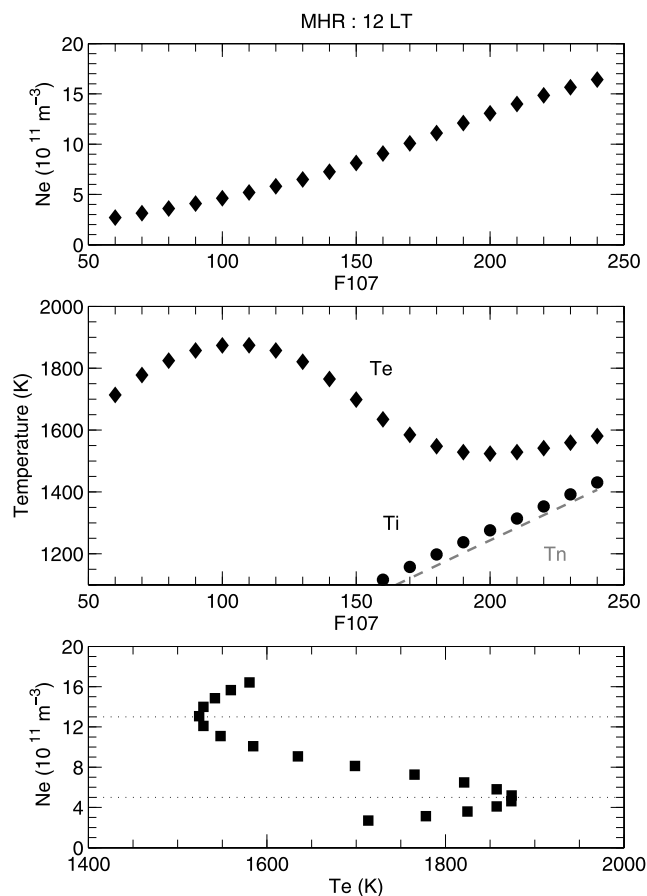


**Figure 6.** The variations of simulated Ne (top), Te (diamonds), Ti (solid circles) and Tn (dashed line) (middle) at the F<sub>2</sub> peak height at Millstone Hill with solar 10.7-cm solar flux F<sub>10.7</sub>, along with the Te-Ne relationship (bottom). F<sub>10.7</sub> is in unit of  $10^{-22}$  W m<sup>-2</sup> Hz<sup>-1</sup>. See the text for more details.

ions is smaller than electron heating rate by solar radiation. The low-energy cooling rate is caused by the relatively low electron densities.

[24] Te then decreases with F<sub>10.7</sub> when F<sub>10.7</sub> values are between  $100 \times 10^{-22}$  and  $180 \times 10^{-22}$  W m<sup>-2</sup> Hz<sup>-1</sup>. Electron densities now are sufficiently high so that the energy loss rate exceeds the photoelectron heating rate because electron cooling rate is proportional to the square of Ne which increases with F<sub>10.7</sub>. When F<sub>10.7</sub> is larger than  $190 \times 10^{-22}$  W m<sup>-2</sup> Hz<sup>-1</sup>, however, Te begins to increase again with F<sub>10.7</sub>. In this case, high electron densities lead to a rapid energy transfer from the electrons to the ions due to the high collision frequencies between them. This results in an enhanced ion temperature that is close to the electron temperature. The high electron or ion densities also result in a fast energy transfer from the ions to the neutrals causing the neutral temperatures to approach to Ti (Figure 6, middle). The net result of this process is the very small temperature differences between the electrons and the ions/neutrals. Thus Te, Ti, and Tn all change in the same way with F<sub>10.7</sub>. Since the total solar heating increases with solar activity, all these temperatures increase with F<sub>10.7</sub>. A quantitative analysis of the relative contributions of individual

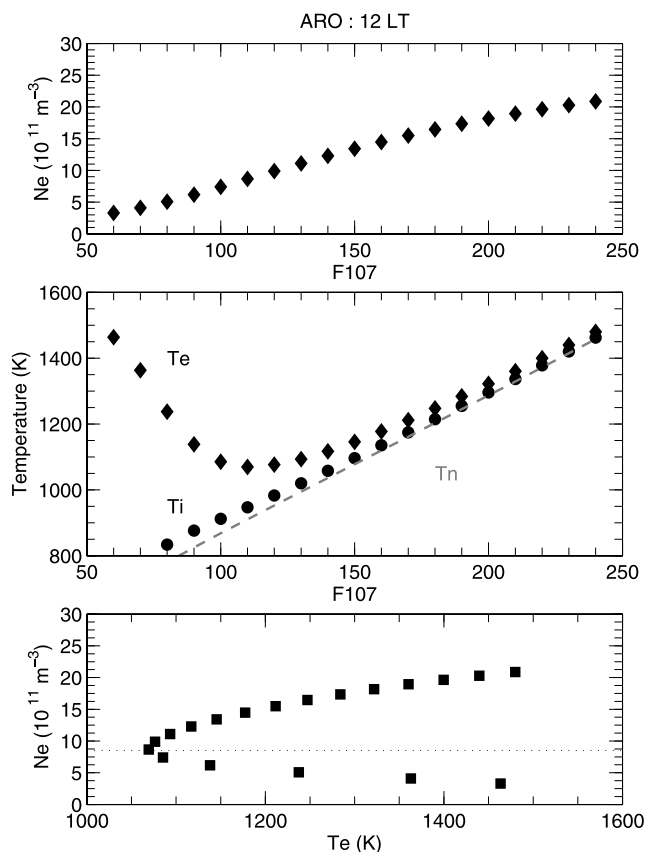


Figure 7. Same as Figure 6, but for Arecibo.

heating and cooling terms to  $T_e$  and their variations with solar activity needs further study.

[25] On the basis of the corresponding values of  $T_e$  and  $N_e$ , we can examine their interrelationship. The increase of  $T_e$  with solar activity basically corresponds to the positive correlation between  $T_e$  and  $N_e$  and vice versa. As shown in Figure 6, it is interesting to note that there exist two  $N_e$  thresholds at about  $5 \times 10^{11}$  and  $13 \times 10^{11} \text{ m}^{-3}$ . Hereafter we call these two  $N_e$  thresholds as the lower and upper thresholds, respectively. The correlation of  $T_e$  and  $N_e$  is negative, when  $N_e$  is intermediate between these two thresholds; the correlation becomes positive when  $N_e$  is lower than the lower threshold or larger than the upper threshold.

[26] Figure 7 depicts the solar variation of daytime  $N_e$  and  $T_e$ , along with their relationship at the F2 peak height at Arecibo.  $N_e$  increases almost linearly with solar activity.  $T_e$  variations are quite different from those at Millstone Hill.  $T_e$  tends to decrease at low solar activity level, and then  $T_e$  increases with solar activity when  $F_{10.7} > 100 \times 10^{-22} \text{ W m}^{-2} \text{ Hz}^{-1}$ . Nevertheless, the variation of  $T_e$  with solar activity can be explained by the same mechanism as that at Millstone Hill. Note that the  $N_e$  increases rapidly with  $F_{10.7}$  at Arecibo and so does the  $N_e^2$ , leading to the domination of electron cooling even at low  $F_{10.7}$  levels. Thus there is no increase of  $T_e$  with solar activity at low  $F_{10.7}$  values as seen at Millstone Hill, resulting in a correlation between  $T_e$  and  $N_e$  that differs from that at Millstone Hill. There only exists an upper  $N_e$  threshold ( $\sim 8.5 \times 10^{11} \text{ m}^{-3}$ ). When  $N_e$  is higher than this upper threshold, the correlation

between  $T_e$  and  $N_e$  is positive and vice versa. It is also reasonable to assume that the occurrence of the threshold varies with local time, season, altitude, and also location.

[27] To validate our simulations, the solar variation of midday  $T_e$  and  $T_i$  from ISR observations at Arecibo at equinox is illuminated in Figure 8. We can see that the observations are consistent with our simulations. The observed  $T_e$  seems to decrease with  $F_{10.7}$  when  $F_{10.7}$  values are lower than  $100 \times 10^{-22} \text{ W m}^{-2} \text{ Hz}^{-1}$ , although the  $T_e$  shows a large scatter. It can be seen clearly that  $T_e$  increases with solar activity when  $F_{10.7} > 100 \times 10^{-22} \text{ W m}^{-2} \text{ Hz}^{-1}$ . As expected, a positive correlation between  $T_e$  and  $N_e$  would occur, the same as the simulations. Furthermore, the solar variation of observed  $T_e$  exhibits the same tendency as that of  $T_i$ , which supports our above explanations. Note that the current IRI model [Bilitza, 2001] cannot predict the solar activity dependence of  $T_e$  (not shown) seen in the observations and simulations because of the fact that the IRI model does not include the  $T_e$  variations with solar activity. Therefore this study can provide a good guidance for developing empirical  $T_e$  model.

[28] The solar activity variations of daytime  $T_e$  at Millstone Hill (Figure 2) and Arecibo (Figure 4) can be explained by the simulations shown in Figures 6–7. At Millstone Hill,  $N_e$  in summer is lower than the lower  $N_e$  threshold; hence  $T_e$  increases with solar activity. Similarly, below  $\sim 300 \text{ km}$  a positive correlation between  $T_e$  and  $N_e$  tends to prevail at both stations. At Arecibo, the upper  $N_e$  threshold usually occurs at low level of  $N_e$ ; therefore a positive correlation prevails in most circumstances.

#### 4.3. Discussion

[29] As seen from our comparisons, the diurnal, seasonal, and solar activity variations of  $T_e$  at Millstone Hill are

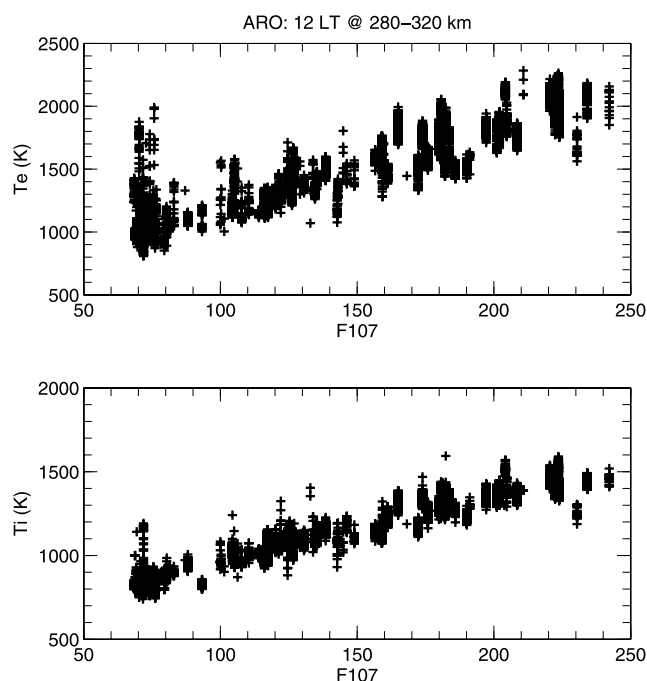
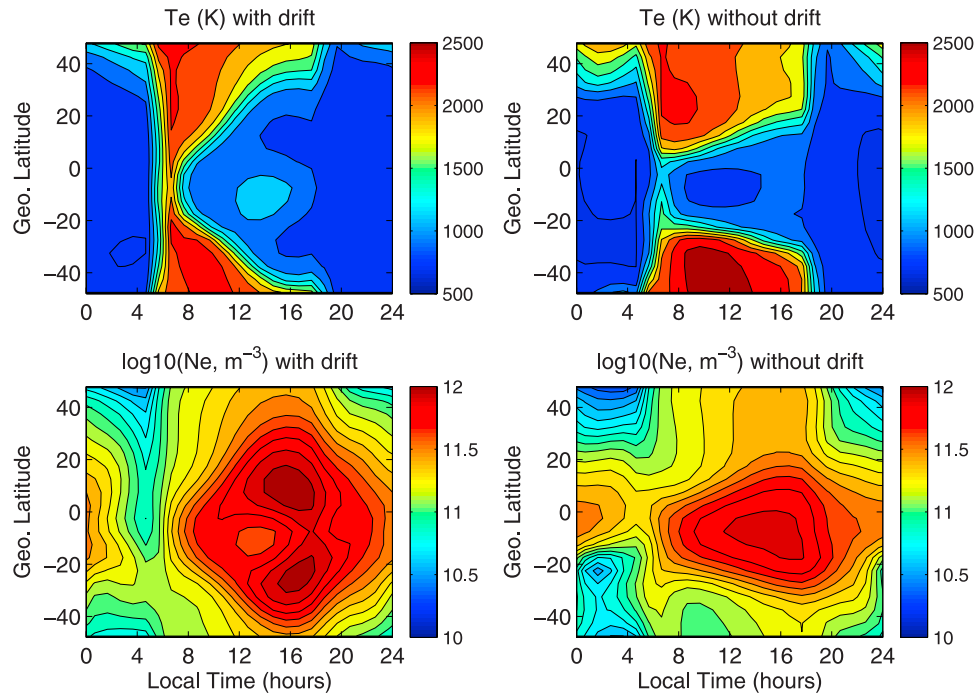


Figure 8. A mass plot showing the variations of the observed  $T_e$  and  $T_i$  at Arecibo with  $F_{10.7}$  in equinox.  $F_{10.7}$  is in unit of  $10^{-22} \text{ W m}^{-2} \text{ Hz}^{-1}$ .



**Figure 9.** Comparison of the modeled Te and Ne variations at 300 km (left) with or (right) without the plasma drift velocity in equinox at low solar activity. The results are shown as functions of geographic latitude and local time for the 65°W longitude. Note the plasma drift effect on producing the morning peak of Te.

different from those at Arecibo. The diurnal variation of Te at Arecibo is characterized by the morning and evening peaks. The morning peak occurs in all seasons and at all solar activity levels, whereas the evening peak only occurs in equinox and winter and at low solar activity. At Millstone Hill, however, the morning peak tends to occur in equinox and winter and at high solar activity, and the evening peak seems to be weak or absent under the considered geophysical conditions. As stated above, the morning peak of Te is caused by the photoelectron heating of the morning low-density electron gas [Dalgarno and McElroy, 1965]. The significant differences between Millstone Hill and Arecibo in the occurrence of the morning peak are related to electron density variations between these two sites and solar zenith angle. At low solar activity, we can see that Ne at Arecibo is much larger (by a factor of about 2) than that at Millstone Hill because Arecibo is located in a low-latitude region and is close to the crest of the equatorial anomaly. So, it would be appropriate to investigate the contribution of the electric field drift to electron density and electron temperature. We run the model again in equinox at low solar activity but without including the electrodynamic effects ( $\mathbf{E} \times \mathbf{B}$ ). As shown in Figure 9, because of the fountain effect caused by the daytime upward drift, the larger Ne gives rise to larger electron cooling, leading to lower Te. When the electric drift is not included in the calculation (Figure 9, right), the crests of the equatorial anomaly of Ne disappears and electron temperature becomes much higher during the daytime, and thus the morning peak becomes less pronounced.

[30] As for the evening peak in Te, it is associated with the photoelectron heating of the low electron density in the evening. Otsuka *et al.* [1998] proposed that the poleward

neutral wind should be responsible for the evening peak at MU. We have checked the predicted neutral wind and found that the maximum meridional wind is only about 15 m/s during 1500–2000 LT and the TIEGCM wind is in good agreement with the FPI wind at Arecibo (not shown). Referring to Figure 1, the heat flux at Arecibo shows an evening peak at low solar activity. However, when we include this peak flux in the calculation, the modeled evening peak is still weak because of the relatively smaller contribution of heat conduction at Arecibo. More realistic  $O^+$  flux changing with neutral wind and temperature is consistently required in order to simulate better the observed features. We are hopeful to solve this question by coupling a plasmasphere model.

[31] A striking feature presented at Arecibo is the daytime Te bulge, characterized by a temperature maximum at altitudes between about 200 and 300 km and a temperature valley (minimum) between 300 and 400 km [Bilitza, 1987]. The temperature valley occurs because the electron cooling by the ions and neutrals exceeds the photoelectron heating. The daytime bulge tends to be prominent at high solar activity because of higher electron densities. On the other hand, the less vertical heat conduction causes the Te daytime bulge to become stronger with decreasing latitude [Otsuka *et al.*, 1998]. In addition, larger photoelectron heating at lower latitudes (where stronger solar irradiation is received) and at high solar activity (when enhanced solar EUV flux would be expected) should also result in a stronger daytime Te bulge. Since the  $F_2$  peak height,  $h_m F_2$ , increases with  $F_{10.7}$  (Figures 3 and 5), electron density does not increase proportionately at the bottomside of  $F_2$  layer as the photoelectron heating does [Sethi *et al.*,

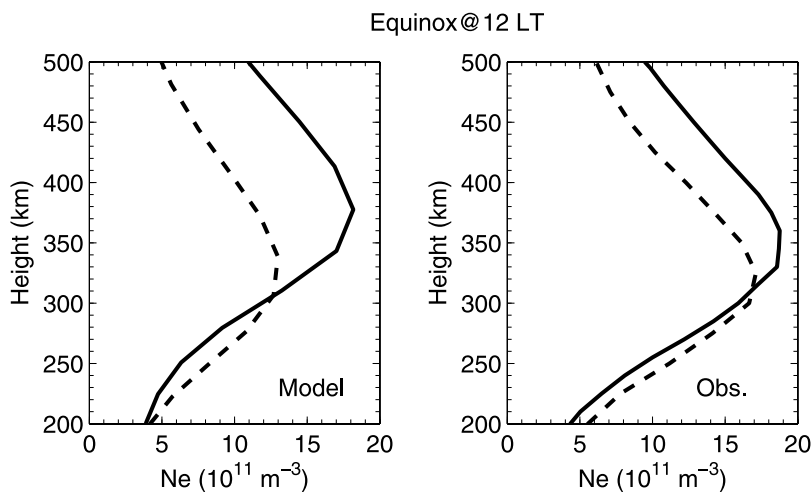


**Figure 10.** Comparison of Ne profiles at Arecibo (solid line) and Millstone Hill (dashed line) at high solar activity. The simulated and observed profiles are shown at left and right, respectively.

2004]. This process also contributes to the prominent daytime Te bulge at high solar activity. As shown in Figure 10, electron densities at the altitudes between  $\sim 200$  and  $300$  km from both the simulations and observations are lower at Arecibo than those at Millstone Hill. This lower electron density at Arecibo, which indicates less loss of heat from the electron gas through collisions with the ions and neutral molecules, in turn produces stronger Te bulge. As mentioned before, the Ne above the  $F_2$  peak height at Arecibo is larger than at Millstone Hill because of the influence of the equatorial anomaly.

## 5. Summary

[32] Long-term ISR electron temperature Te measurements for more than two solar cycles at Millstone Hill (1976–2002) and Arecibo (1966–2002) have been used to compare with theoretical results from the TIEGCM to investigate the temporal variations of Te and their altitude and latitudinal dependencies. A comprehensive picture of the diurnal, seasonal, and solar activity variations of observed and simulated Te has been presented. Overall, the diurnal, seasonal, and solar activity variations of Te can be interpreted in terms of the corresponding variations of the electron density. The main conclusions are drawn as follows:

[33] 1. At Millstone Hill, both the model and observations show that the morning peak tends to occur in equinox and winter and at high solar activity, whereas the evening peak seems to be weak or absent. At Arecibo, the diurnal variation of observed Te is characterized by the morning and evening peaks; the morning peak occurs in all seasons and at all solar activity levels, whereas the evening peak only occurs in equinox and winter and at low solar activity. The model reproduces well the morning peak although the modeled evening peak is much weaker. The significant morning peak at low solar activity over Arecibo is associated with the equatorial anomaly that results in a large electron density and low Te in the noon and afternoon sectors.

[34] 2. The model calculations show that the daytime bulge of Te tends to occur at lower latitude (Arecibo) and

high solar activity, the same as the observations. Further study suggests that in addition to effects of heat conduction, the changes of photoelectron heating and the electron density of the  $F$  layer with solar activity also contribute to the latitudinal and solar activity dependence of the Te bulge.

[35] 3. The solar activity variation of Te depends on the local time, season, and altitude. At both stations, Te tends to increase with solar activity during the daytime below  $\sim 300$  km, and at the nighttime at all altitudes except for the winter nighttime at Millstone Hill when the magnetic conjugate point is still sunlit. Above  $300$  km, Te increases with solar activity in equinox and summer at Arecibo, while it does so only in summer at Millstone Hill. The model can capture well these solar activity features except for the evening period at Arecibo when the evening peak occurs.

[36] 4. Further simulations reveal that ionospheric electron gas exhibits a complex thermal response to solar activity. At Millstone Hill, when  $F_{10.7}$  values are less than  $100 \times 10^{-22} \text{ W m}^{-2} \text{ Hz}^{-1}$  or larger than  $190 \times 10^{-22} \text{ W m}^{-2} \text{ Hz}^{-1}$ , the midday Te at the  $F_2$  peak height tends to increase with solar activity; so does at Arecibo when  $F_{10.7}$  values are larger than  $100 \times 10^{-22} \text{ W m}^{-2} \text{ Hz}^{-1}$ . Correspondingly, a positive correlation between Te and Ne happens under these circumstances. An anticorrection between daytime Te and Ne occurs only in a certain range of Ne. This study is the first to illustrate these interesting features using a comprehensive first-principles theoretical model. Therefore our simulations can provide a good reference for empirical model development and data analysis.

[37] **Acknowledgments.** NCAR is supported by the National Science Foundation. We would like to thank Art Richmond, Alan G. Burns, and C. G. Fesen for useful discussions. The Millstone Hill incoherent scatter radar is supported by a cooperative agreement between the U.S. National Science Foundation and the Massachusetts Institute of Technology. The Arecibo Observatory is the principal facility of the U.S. National Astronomy and Ionosphere Center, which is operated by the Cornell University under a cooperative agreement with the National Science Foundation. The Arecibo ISR data are taken from the CEDAR database at NCAR, which is supported by the National Science Foundation.

[38] Zuyin Pu thanks Yuichi Otsuka and another reviewer for their assistance in evaluating this paper.

## References

- Banks, P. M., and G. Kocharts (1973), *Aeronomy*, Elsevier, New York.
- Bilitza, D. (1975), Models for the relationship between electron density and temperature in the upper ionosphere, *J. Atmos. Terr. Phys.*, *37*, 1219–1222.
- Bilitza, D. (1987), Description of the mean behaviour of ionospheric plasma temperatures, *Adv. Space Res.*, *7*, 93–98.
- Bilitza, D. (2001), International reference ionosphere 2000, *Radio Sci.*, *36*(2), 261–275.
- Bilitza, D., and W. R. Hoegy (1990), Solar activity variations of ionospheric plasma temperatures, *Adv. Space Res.*, *10*, 81–90.
- Brace, L. H., and R. F. Theis (1978), An empirical model of the interrelationship of electron temperature and density in the daytime thermosphere at solar minimum, *Geophys. Res. Lett.*, *5*, 275–278.
- Brace, L. H., and R. F. Theis (1981), Global empirical models of ionospheric electron temperature in the upper *F*-region and plasmasphere based on in situ measurements from the Atmosphere Explorer-C, ISIS-1 and ISIS-2 Satellites, *J. Atmos. Terr. Phys.*, *43*, 1317–1347.
- Buonsanto, M. J. (1989), Comparison of incoherent scatter observations of electron density, and electron and ion temperature at Millstone Hill with the International Reference Ionosphere, *J. Atmos. Terr. Phys.*, *51*, 441–468.
- Dalgarno, A., and M. B. McElroy (1965), Ionosphere electron temperatures near Dawn, *Planet. Space Sci.*, *13*, 143–145.
- Evans, J. V. (1967), Midlatitude electron and ion temperatures at sunspot minimum, *Planet. Space Sci.*, *15*, 1557–1570.
- Evans, J. V. (1973), Seasonal and sunspot cycle variation of *F* region electron temperatures and protonospheric heat flux, *J. Geophys. Res.*, *78*, 2344–2349.
- Fesen, C. G., D. L. Hysell, J. M. Meriwether, M. Mendillo, B. G. Fejer, R. G. Roble, B. W. Reinisch, and M. A. Biondi (2002), Modeling the low-latitude thermosphere and ionosphere, *J. Atmos. Sol. Terr. Phys.*, *64*, 1337–1349.
- Fukao, S., W. L. Oliver, Y. Onishi, T. Takami, T. Sato, T. Tsuda, M. Yamamoto, and S. Kato (1991), *F*-region seasonal behavior as measured by the MU radar, *J. Atmos. Terr. Phys.*, *53*, 599–618.
- Hagan, M. E., M. D. Burrage, J. M. Forbes, J. Hackney, W. J. Randel, and X. Zhang (1999), GSWM-98: Results for migrating solar tides, *J. Geophys. Res.*, *104*, 6813–6828.
- Hierl, P. M., I. Dotan, and A. A. Viggiano (1997), Rate constants for the reactions of  $O^+$  with  $N_2$  and  $O_2$  as a function of temperature (300–1899 K), *J. Chem. Phys.*, *106*, 3540–3544.
- Holt, J. M., S.-R. Zhang, and M. J. Buonsanto (2002), Regional and local ionospheric models based on Millstone Hill incoherent scatter radar data, *Geophys. Res. Lett.*, *29*(9), 1358, doi:10.1029/2001GL013579.
- Lei, J., L. Liu, W. Wan, and S.-R. Zhang (2005), Variations of electron density based on long-term incoherent scatter radar and ionosonde measurements over Millstone Hill, *Radio Sci.*, *40*, RS2008, doi:10.1029/2004RS003106.
- Mahajan, K. K. (1977), Models of electron temperature in the ionospheric *F*-region using electron density height profiles, *J. Atmos. Terr. Phys.*, *39*, 637–639.
- Oliver, W. L., T. Takami, S. Fukao, T. Sato, M. Yamamoto, T. Tsuda, T. Nakamura, and S. Kato (1991), Measurements of ionospheric and thermospheric temperatures and densities with the Middle and Upper Atmosphere Radar, *J. Geophys. Res.*, *96*, 17,827–17,838.
- Otsuka, Y., S. Kawamura, N. Balan, S. Fukao, and G. J. Bailey (1998), Plasma temperature variations in the ionosphere over the middle and upper atmosphere radar, *J. Geophys. Res.*, *103*, 20,705–20,713.
- Oyama, K.-I., S. Watanabe, Y. Su, T. Takahashi, and K. Hirao (1996), Seasonal, local time, and longitude variations of electron temperature at the height of 600 km in the low latitude region, *Adv. Space Res.*, *18*, 269–278.
- Oyama, K.-I., M. A. Abdu, N. Balan, G. J. Bailey, S. Watanabe, T. Takahashi, E. R. de Paula, I. S. Batista, F. Isoda, and H. Oya (1997), High electron temperature associated with the prereversal enhancement in the equatorial ionosphere, *J. Geophys. Res.*, *102*, 417–424.
- Prabhakaran Nayar, S. R., et al. (2004), Study of the evolution of Te and Ti at the low-latitude upper ionosphere using SROSS-C2 RPA observations, *J. Atmos. Sol. Terr. Phys.*, *66*, 1075–1083.
- Richmond, A. D., E. C. Ridley, and R. G. Roble (1992), A thermosphere/ionosphere general circulation model with coupled electrodynamics, *Geophys. Res. Lett.*, *19*, 601–604.
- Roble, R. G. (1975), The calculated and observed diurnal variation of the ionosphere over Millstone Hill on 23–24 March 1970, *Planet. Space Sci.*, *23*, 1017–1030.
- Roble, R. G. (1995), Energetics of the mesosphere and thermosphere, in *The Upper Mesosphere and Lower Thermosphere: A Review of Experiment and Theory*, *Geophys. Monogr. Ser.*, vol. 87, edited by R. M. Johnson and T. L. Killeen, pp. 1–21, AGU, Washington, D. C.
- Roble, R. G., and E. C. Ridley (1987), An auroral model for the NCAR thermospheric general circulation model (TGCM), *Ann. Geophys.*, *5*, 369–382.
- Schunk, R. W., and A. F. Nagy (1978), Electron temperatures in the *F* region ionosphere: Theory and observations, *Rev. Geophys.*, *16*, 355–399.
- Sethi, N. K., V. K. Pandey, and K. K. Mahajan (2004), Seasonal and solar activity changes of electron temperature in the *F*-region and topside ionosphere, *Adv. Space Res.*, *33*, 970–974.
- Sharma, D. K., J. Rai, M. Israil, and P. Subrahmanyam (2005), Diurnal, seasonal and latitudinal variation of ionospheric temperatures of the topside *F* region over Indian region during solar minimum year (1995–1996), *J. Atmos. Sol. Terr. Phys.*, *67*, 269–274.
- Solomon, S. C., and L. Qian (2005), Solar extreme-ultraviolet irradiance for general circulation models, *J. Geophys. Res.*, *110*, A10306, doi:10.1029/2005JA011160.
- Su, Y. Z., K.-I. Oyama, G. J. Bailey, S. Fukao, T. Takahashi, and H. Oya (1996), Longitudinal variations of the topside ionosphere at low latitudes: Satellite measurements and mathematical modeling, *J. Geophys. Res.*, *101*, 17,191–17,205.
- Venkatraman, S., and R. Heelis (1999), Longitudinal and seasonal variations in nighttime plasma temperatures in the equatorial topside ionosphere during solar maximum, *J. Geophys. Res.*, *104*, 2603–2611.
- Wang, W., A. G. Burns, and T. L. Killeen (2006), A numerical study of the response of ionospheric temperature on geomagnetic activity, *J. Geophys. Res.*, *111*, A11301, doi:10.1029/2006JA011698.
- Watanabe, S., and K.-I. Oyama (1996), Effect of neutral wind on the electron temperature at a height of 600 km in the low-latitude region, *Ann. Geophys.*, *14*, 290–296.
- Zhang, S.-R., and J. M. Holt (2004), Ionospheric plasma temperatures during 1976–2001 over Millstone Hill, *Adv. Space Res.*, *33*, 963–969.
- Zhang, S.-R., J. M. Holt, A. M. Zaluca, and C. Amory-Mazaudier (2004), Midlatitude ionospheric plasma temperature climatology and empirical model based on Saint Santin incoherent scatter radar data from 1966 to 1987, *J. Geophys. Res.*, *109*, A11311, doi:10.1029/2004JA010709.

B. A. Emery, J. Lei, R. G. Roble, and W. Wang, High Altitude Observatory, National Center for Atmospheric Research, 3080 Center Green, Boulder, CO 80301, USA. (leijh@ucar.edu)

S.-R. Zhang, Haystack Observatory, Massachusetts Institute of Technology, Route 40, Westford, MA 01886, USA.